CORROSION RESISTANCE OF AZ31 MAGNESIUM ALLOY INFLUENCED BY CONVENTIONAL CUTTING FLUID

Daniel Kajánek[1,2*], Filip Pastorek[2], Branislav Hadzima[2]

[1] Department of Materials Engineering, Faculty of Mechanical Engineering, University of Žilina, Univerzitná 1, 010 26 Žilina, Slovak Republic.
[2] Research Centre, University of Žilina, Univerzitná 1, 010 26 Žilina, Slovak Republic.
[*]corresponding author: e-mail: kajanek@fstroj.uniza.sk, tel: 00421415132624

Resume
This paper deals with the evaluation of cutting fluid impact on corrosion resistance of AZ31 magnesium alloy in aggressive environment containing chloride ions supported by photo documentation. Ground samples were immersed in the standard commercial cutting fluid for 5 minutes to simulate conditions during machining process at the temperature of 22 ± 2 °C and subsequently cleaned and immersed in 0.1M NaCl solution at the temperature of 22 ± 2°C in order to measure electrochemical corrosion characteristics. Cyclic potentiodynamic polarization (CPP) tests were chosen as a testing method. The measured CPP curves of immersed samples and ground samples were analysed by Tafel extrapolation method. The values of obtained electrochemical characteristics show that the chosen cutting fluid has negative effect on corrosion resistance of AZ31 magnesium alloy in sodium chloride solution.

Article info
Article history:
Received 23 July 2017
Accepted 19 October 2017
Online 02 January 2018

Keywords:
Magnesium alloy;
Corrosion;
Cutting fluid;
Cyclic potentiodynamic polarization test.

Available online: http://fstroj.uniza.sk/journal-mi/PDF/2017/08-2017.pdf

ISSN 1335-0803 (print version)
ISSN 1338-6174 (online version)

1. Introduction

In the modern world engineering, there is a need to reduce the weight of the components and machines (cars, aircrafts, ships, etc.) with the aim to lower operational costs, fuel consumption and also limits the carbon footprint. Magnesium and its alloys represents one of the few possibilities to accede this requirement. These alloys belong to the category of progressive materials used in automotive and aircraft industry due to the many outstanding properties, e.g. low weight, high specific strength, high dumping capacity and good machinability. From the ecological point of view, they are recyclable and after the end of their lifetime they could be used as a sacrificial anode to protect another metal [1 - 6, 13]. The Mg-Al-Zn alloys exhibit good combination of mechanical properties, castability, biocompatibility, workability and because of that they are extensively used by the engineers. The AZ31 alloy shows good plasticity, weldability, corrosion resistance, can withstand small loads and such that is often used in aircraft industry for exemplatory brackets and small components. According to the various authors alloy also provides very good biodegradable properties [7 - 9]. Despite of these pros, there is problem with high reactivity of Mg alloys which leads to the lower corrosion resistance compared to the aluminium alloys or steels and limits their wider usage [10, 11]. The Mg alloys reacts briefly when they are exposed to corrosive environment (aerial or aqueous) and the Mg oxides (MgO) or hydroxides $Mg(OH)_2$ are formed on the surface. These substances are not stable in the acidic or neutral conditions and such that do not protect the magnesium parts [12 - 14]. During the most of the machining processes, the magnesium workpiece is in contact with the cutting fluid. The components

of the conventional cutting fluid could react with the alloy which may lead to the decrease of corrosion resistance.

This contribution is focused on the evaluation of the conventional cutting fluid impact on the corrosion resistance of the AZ31 magnesium alloy.

2. Experimental material and methods

The AZ31 magnesium alloy prepared by continual casting and homogenized at the temperature of 420 °C for 6 h has been used as an experimental material. Its chemical composition given by the material list is mentioned in the Table 1. The samples used for the metallographic observation have been prepared according to the standard metallographic procedures used for the Mg alloys. Subsequently, the samples have been etched by the etchant consists of acetic acid, picric acid, demineralised water and ethanol [15]. The microstructure of AZ31 samples has been observed using light microscope ZEISS Axio Imager.Z1M.

The samples have been ground before immersion to the cutting fluid by an emery paper p1000 to ensure the same surface roughness [16]. In the next step, they have been submerged to the conventional cutting emulsion with pH 9 for the 5 minute to simulate the conditions during the machining process. After that, the samples were cleaned by the demineralised water, ethanol and dried by the steam of air. The used cutting fluid consists of mineral oils, additives and dangerous components which are listed in the Table 2. For the better interpretation of the results, the photo documentation of the samples surfaces before and after the immersion has been done on the stereomicroscope OLYMPUS SZX16.

The cyclic potentiodynamic polarization (CPP) tests have been chosen for evaluation of the electrochemical corrosion characteristics. The measurements have been performed in the 0.1M NaCl (aggressive aqueous environment containing chlorides) with pH 7.2 at the temperature of 22 ± 2 °C using laboratory potentiostat VSP Biologic SAS [17]. The three electrode cell system has been used including AZ31 sample with the exposed area of 1 cm^2 set as working electrode, platinum electrode set as a counter and saturated calomel electrode which served as a reference electrode (+0.242 V vs. SHE). The CPP tests start after 5 minute of potential stabilization between the AZ31 sample and testing electrolyte. The applied potential ranged from -150 mV to +400 mV in order to record pitting potential area. The range of potentials has been set with respect to open circuit potential (OCP) and the scan rate was 1 $mV.s^{-1}$. The measured data in form of cyclic potentiodynamic curves have been analysed by the Tafel extrapolation method and owing to that values of corrosion potential E_{corr} and corrosion current density i_{corr} have been obtained using EC Lab V10.34 software. From the E_{corr} and i_{corr} values the corrosion rate r_{corr} has been calculated.

Table 1

Chemical composition of AZ31 magnesium alloy.

Component	Al	Zn	Mn	Si	Cu	Fe	Mg
wt. %	2.96	0.82	0.43	0.004	0.004	0.002	balance

Table 2

Dangerous component of conventional cutting fluid

Component	Amine soap	Methylene dimorpoholine	Alcohol C16-18, C18	Polyglycoether	Boracic Acid	Neutralized KOH
wt. %	10 - 20	1 - 5	1 - 5	1 - 5	1 - 5	0.002

3. Results and Discussion

The microstructure of AZ31 magnesium alloy (Fig. 1) consists of polyedral grains of solid solution of aluminium, zinc and other alloying elements in magnesium. There are visible twins and areas of $Al_{12}Mg_{17}$ intermetallic phase.

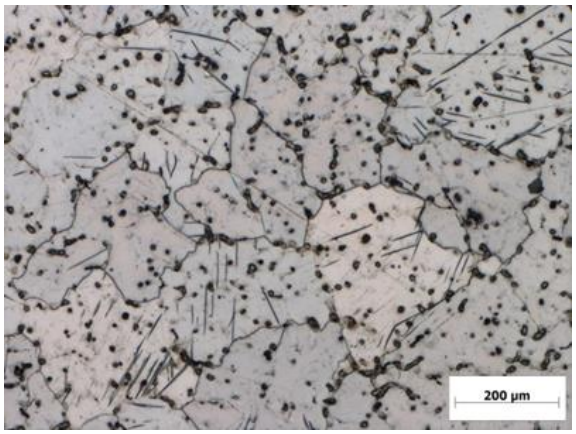

Fig. 1. Microstructure of AZ31 magnesium alloy. (full colour version available online)

The surface of the ground AZ31 sample and sample after immersion is depicted in the Fig. 2. It can be seen that the immersion in cutting fluid leads to the creation of corrosion products layer due to the reaction of Mg sample with components contained in fluid. Another components are MgO and $Mg(OH)_2$ probably formed on the surface due to the aqueous character of the fluid [18].

Measured CPP curves of AZ31 tested samples in 0.1M NaCl are shown in Fig. 3. The values of electrochemical characteristics obtained by the Tafel extrapolation method for both states are listed in Table 3. The samples in ground state have reached (in direct polarization) the corrosion potential E_{corr} value of -1561 mV and value of corrosion current density of 5.3 $\mu A.cm^{-2}$. It can be seen that after the backward polarization, ground AZ31 samples exhibit more negative corrosion potential and higher corrosion current density due to the breakdown of the surface film probably consisting of $Mg(OH)_2$ occurred at the pitting potential E_{pt} (-1429 mV). During the exposition in aqueous environment following reaction takes place: $MgO + H_2O \rightarrow Mg(OH)_2$. According the E-pH diagram for magnesium in water environment, $Mg(OH)_2$ is stable only in strongly alkaline environments. The ground samples tented to corrode rapidly after the breakdown of the surface film due to its interaction with aggressive chloride ions Cl^- contained in the testing electrolyte [12]. As can be seen from electrochemical characteristics mentioned in Table 3, the samples influenced by the immersion in cutting fluid have reached more positive value of E_{corr} (-1391 mV) compared to the ground samples. On the other hand, the corrosion current density increased to the value of 90.6 $\mu A.cm^{-2}$. This value is more than 17-times higher in comparison with the i_{corr} of ground AZ31 samples. The part of CPP curve measured during the backward polarization shows the shift of E_{corr} to the more negative value and higher i_{corr}. It has to be noted that this backward E_{corr} is still more positive compared to the direct E_{corr} of the ground samples. The fact that the influenced samples exhibit more positive values of corrosion potential means that the presence of film created on surface during immersion in cutting fluid leads to the thermodynamically nobler behaviour of these samples. In terms of corrosion kinetics, the significantly higher corrosion current density values of influenced samples means that corrosion rate is higher compared to non-influenced ones as it is shown in Table 3. This fact is probably caused by the non-protective and highly soluble layer of corrosion products consisted of $MgCl_2$ and $Mg(OH)_2$ created on the AZ31 surface which are unstable when exposed to the Cl^- ions and such that provide poor corrosion protection to the magnesium substrate.

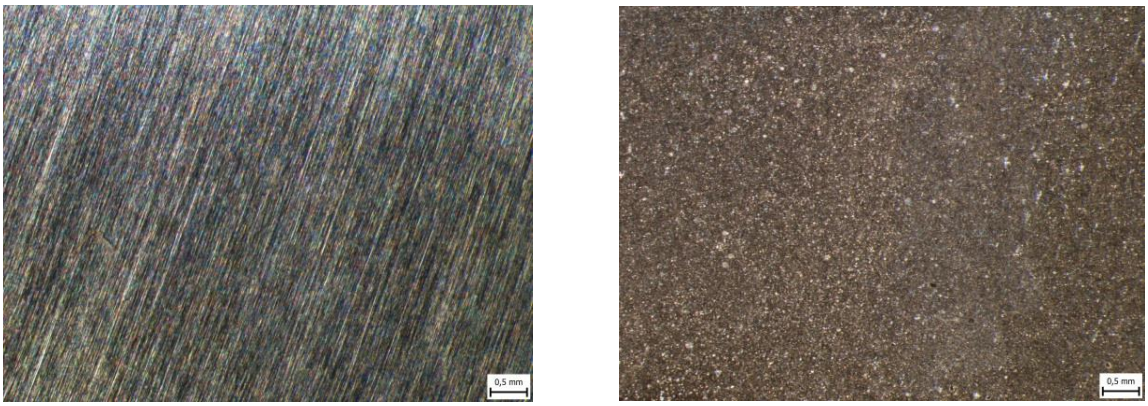

a) ground sample *b) after immersion in cutting fluid*

Fig. 2. Surface of the AZ31.
(full colour version available online)

Table 3

Electrochemical characteristics of the ground samples and samples influenced by the immersion in cutting fluid measure in 0.1M NaCl.

	E_{corr} (mV)	i_{corr} (μA/cm^2)	β_a (mV/dec.)	β_c (mV/dec.)	r_{corr} (mm/year)
Ground	-1561±21	5.3±0.1	121±7	119±6	0.12±0.01
Influenced by cutting fluid	-1391±10	90.6±3.6	131±11	233±21	2.1±0.2

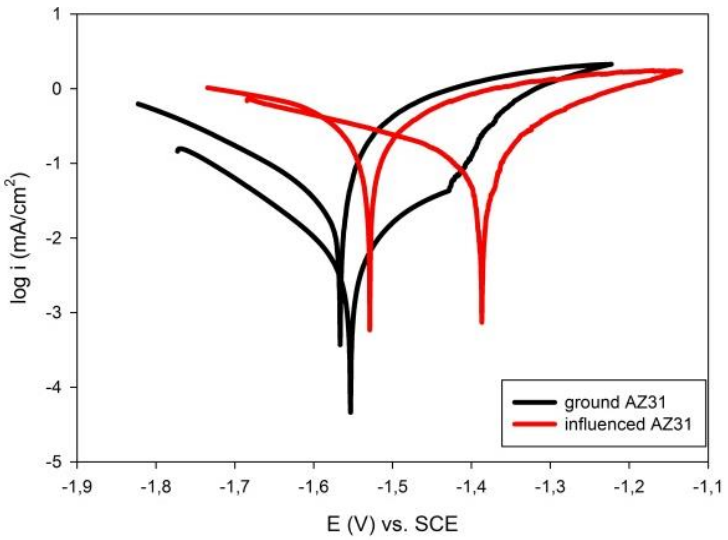

Fig. 3. Cyclic potentiodynamic polarization curves for the ground and influenced AZ31 Mg alloy in 0.1M NaCl.
(full colour version available online)

4. Conclusions

According to the experiments and analysis that have been done, it can be concluded that the immersion in conventional cutting fluid leads to the creation of surface film on the AZ31 Mg alloy samples due to the interaction of fluid components with Mg substrate. The performed CPP measurements in 0.1M NaCl shows that the cutting fluid positively influenced thermodynamic stability of samples as the values of corrosion potential have been more positive to the values

of the ground samples and it means that influenced samples are thermodynamically more stable. However, the corrosion current density increased 17-times after impact of cutting fluid. From the corrosion kinetics point of view, it means that the corrosion rate is higher after the immersion in cutting fluid as the corrosion current density is in direct proportionality with corrosion rate. This negative influence on corrosion behaviour in environment containing Cl^- could be overcome by the using of cutting fluid with more suitable chemical composition that does not react with the Mg surface or by the usage of proper removing technique of the created surface film.

Acknowledgements

The research is supported by the ERDF and Slovak state budget, projects No. ITMS 26220220048, ITMS 26220220121 and by Slovak Grant Agency by the project No. VEGA 1/0045/17.

References

[1] J. Drábiková, F. Pastorek, S. Fintová, P. Doležal, J. Wasserbauer: Koroze a ochrana materiálu 60(5) (2016) 132-138.

[2] J.E. Gray, B. Luan: J. Alloys Compd. 336(1) (2002) 88-113.

[3] J. Liao, M. Hotta: Corros. Sci. 100 (2015) 353-364.

[4] Y. Zhao, G.Wu, H. Pan, K.W.K. Yeung, P.K. Chu: Mater. Chem. and Phys. 132(1) (2012) 187-191.

[5] Y. Gu, S. Bandopadhyay, Ch. Chen, Ch. Ning, Y. Guo: Materials and Design 43 (2013) 66-75.

[6] B. Hadzima, P. Palček, M. Chalupová, R. Čanády: Kovové materiály 41 (4) (2003) 257-269.

[7] H. Feng et al.: J. Alloys Compd. 695 (2017) 2330-2338.

[8] S.S. Jamali: Corros. Sci. 86 (2014) 93-100.

[9] A. Dziubinska, A. Gontarz, K. Horzelska, P. Piesko: Proceedia Manufacturing 2 (2015) 337-341.

[10] Y. Su et al.: Surface and Coatings Technology 307(A) (2016) 99-108.

[11] M. Mhaede, F. Pastorek, B. Hadzima: Mater. Sci. Eng. C 39 (2014) 330-335.

[12] G.L. Song: Advanced Materials Engineering 7(7) (2005) 563-586.

[13] Y. Yang, F. Scenini, M. Curioni: Electrochimica acta 198 (2016) 174-184.

[14] M. Esmaily et al.: Progress in Materials Science 89 (2017) 92-193.

[15] G.F.V. Voort: ASM Handbook: Metalography and Microstructures, 9th edition, ASM International, Almere 2004.

[16] F. Pastorek, B. Hadzima: Mater. Eng. – Mater. Inž. 20(2) (2013) 54-63.

[17] K. Arakami, T. Shimura: Corros. Sci. 52(4) (2010) 1464-1471.

[18] M. Danaiae, R.M. Asmussen, P. Jakupi, D.W. Shoesmith, G.A. Botton: Corros. Sci. 77 (2013) 151-163.

CHARACTERIZATION OF UNCONVENTIONAL FLUORIDE CONVERSION COATING PREPARED ON AZ31 MAGNESIUM ALLOY

Juliána Drábiková[1*], Stanislava Fintová[1,2], Pavel Doležal[1,3], Jaromír Wasserbauer[1], Petr Ptáček[1]

[1] Centre of Materials Research, Faculty of Chemistry, Brno University of Technology, Purkyňova 464/118, 612 00 Brno, Czech Republic.
[2] Institute of Physics of Materials, Academy of Sciences of the Czech Republic, v. v. i., Žižkova 22, 616 62 Brno, Czech Republic.
[3] Institute of Materials Science and Engineering, Faculty of Mechanical Engineering, Brno University of Technology, Technická 2896/2, 616 69 Brno, Czech Republic
[*]corresponding author: e-mail: xcdrabikovaj@fch.vut.cz

Resume
Appropriate chemical composition of some magnesium alloys allows their application in biomedical field. However, the high reactivity of magnesium is a limiting factor for magnesium based material application due to the low corrosion resistance. Fluoride conversion coatings were shown to be appropriate barrier increasing magnesium corrosion resistance and providing biocompatibility. Besides good corrosion resistance and bio-properties also material wear resistance is an important factor for the biomedical implants due to their implementation into the human body. The paper offers methodology for creation of fluoride conversion coating from $Na[BF_4]$ salt melt at 450 °C including coatings characterization in terms of morphology, coverage and scratch test. Increasing the coating time the increase of the coating thickness and resistance to wear was observed.

Available online: http://fstroj.uniza.sk/journal-mi/PDF/2017/09-2017.pdf

Article info
Article history:
Received 20 October 2017
Accepted 23 December 2017
Online 02 January 2018

Keywords:
Magnesium alloy;
Fluoride conversion coating;
Scratch test.

ISSN 1335-0803 (print version)
ISSN 1338-6174 (online version)

1. Introduction

Low toxicity and biocompatibility are the basic properties required on the material for medical applications. Magnesium and many of its alloys meet the requirements for implants and even provide biodegradation [1, 2]. Biodegradation is an advantage over conventional metallic material for medical applications such as stainless steels, Ti and Co alloys, while the implant does not have to be surgically removed after the healing. However, due to the high Mg reactivity, the biodegradation is too fast in the bio-environment and the material does not provide sufficient support to the bone or tissues. Also, the degradation of Mg is accompanied by the creation of hydrogen [2 - 4].

Application of coatings is one of the most effective surface treatment methods improving material corrosion resistance. Besides the adequate properties of the metallic implant material, also the coating have to meet requirements of the medical field. Fluoride conversion coatings were shown to be effective to improve Mg-based material corrosion resistance while the coatings are acceptable for the human body and can even positively affect the healing process. Conventional fluoride conversion coatings preparation is based on the dipping of the material into HF solution at a defined temperature for a specific time [5 - 9]. Unconventional coating preparation was presented in [10, 11] while a positive influence on material electrochemical corrosion properties was presented in [9, 11]. Unconventional preparation technique was based on the dipping of the material into the melt of $Na[BF_4]$ salt at elevated temperature.

The coating prepared from the salt melt consists of primary MgF_2 layer and secondary $NaMgF_3$ layer, which is soluble in boiling water [9, 11]. The electrochemical corrosion characteristics of the MgF_2 coating were shown to be higher for the materials coated in $Na[BF_4]$ salt melt at 450 °C when compared to the conventionally coated materials dipped into HF solution in [9].

However, not only the bio-acceptance of the coating is important in the case of implants. Also, the wear resistance of the coating is important to ensure the not damaged surface of the implant after implementation of the implant to the human body.

The presented paper is aimed at the preparation and characterization of the unconventional fluoride conversion coating via dipping of the AZ31 magnesium alloy specimens into the $Na[BF_4]$ salt melt at 450 °C for the different treatment time. The used treatment times were 0.5, 2 and 8 h. The prepared coatings were analyzed in terms of scanning electron microscopy and scratch test.

2. Experimental material and procedure

2.1 Experimental material

AZ31 wrought magnesium alloy was used as the experimental material for fluoride conversion coating preparation. Magnesium alloy was delivered in the form of a sheet. Typical microstructure of the alloy consisting of polyhedral grains of the solid solution of alloying elements in magnesium is shown in Fig. 1. Average grains size was determined by the linear method as 14.5 ± 0.4 μm. In the microstructure was observed also the presence of the uniformly distributed small amount of Al-Mn based intermetallic phase particles.

Microstructural analysis of the experimental material was performed on specimens prepared by conventional metallographic procedure consisting of grinding (SiC papers no. 1200 and 4000), polishing (diamond pastes 3, 1 and 0.25 μm) using isopropanol as the cooling medium and etching by picral (35 ml ethanol + 5 ml distilled water + 5 ml concentrated acetic acid + 2.1g picric acid).

Examination of the experimental material microstructure used for the grain size determination and intermetallic phase particles distribution within the microstructure was performed using Zeiss Axio Observer Z1 light optical microscope (LM). Jeol JSM-7600F scanning electron microscope (SEM) was used for a detailed analysis of the experimental material microstructural features and energy-dispersive X-ray spectroscopy (EDS) was used for chemical analysis of present intermetallic phases.

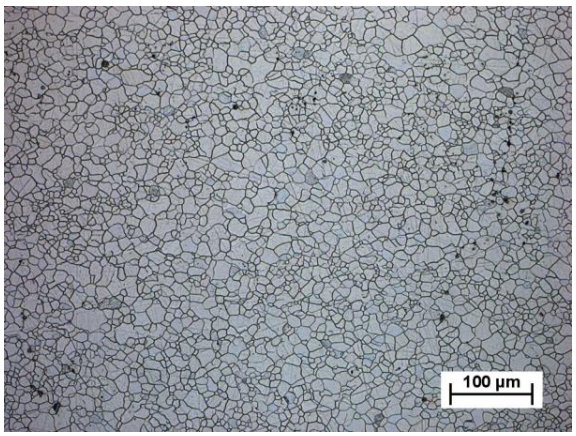

a) as-received microstructure, LM

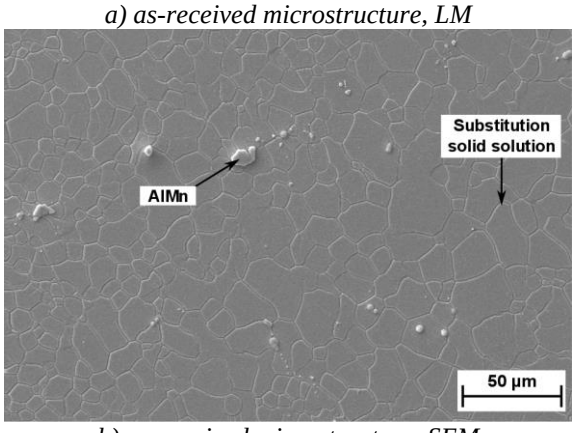

b) as-received microstructure, SEM

Fig. 1. Typical microstructure of AZ31 wrought magnesium alloy.

2.2 Coating preparation and characterization

Fluoride conversion coating was prepared on specimens of wrought AZ31 magnesium

alloy with the dimensions of 20×20×1.45 mm. Polished specimens were after grinding on SiC papers (no. 1200 and 4000) polished on diamond pastes (3, 1 and 0.25 μm) using isopropanol until an uniform mirror-like surface without evident scratches was reached. All the specimens were cleaned with isopropanol and dried by hot air after surface finishing.

Conversion coating was prepared by chemical reaction of the coated material and $Na[BF_4]$ salt melt at the temperature of 450 °C. An amount of 130 g of $Na[BF_4]$ salt was sprinkled to the corundum crucible with a diameter of 40 mm and 60 mm high and melted in an electric furnace for 2 h.

AZ31 specimens were dipped into $Na[BF_4]$ molten salt for various treatment times: 0.5, 2 and 8 h. After the coating preparation, the specimens were removed from the salt melt and subsequently dipped in the boiling distilled water for 10 min. Boiling of the specimens in the distilled water removed the salt residuals.

Surface morphology of the prepared coatings was determined using SEM. Coatings thickness and homogeneity within the coating cross-section were estimated using SEM.

2.3 Scratch test

Specimens coated in $Na[BF_4]$ salt melt for 0.5, 2 and 8 h were subjected to scratch tests. REVETEST Scratch Testing system with acoustic emission detector was used to perform fluoride conversion coating adhesion behavior. Loading increasing from 1 to 20 N (progressive mode) with the increment of 10 $N \cdot min^{-1}$ was used to test coatings properties. In the case of the 0.5 h coating preparation time, only 10 N load was used due to the low coating thickness. On each specimen, a scratch with a length of 3 mm was created. Created scratches were documented on Stemi 2000-C light optical microscope and detailed analysis of the coating damage was performed using SEM.

3. Results

3.1 Coating characteristics

Dipping of the AZ31 polished specimens to the $Na[BF_4]$ molten salt for the different time resulted in a creation of uniform fluoride conversion coating.

Observations of the coatings surface revealed some structural defects on the coatings surface and increasing relief of the coating defect by increasing treatment time. The surface of specimens supposed to the scratch test is shown in Fig. 2.

Structural defects and surface waviness were characteristic features for all the coatings.

SEM analysis of the coated specimen cross-sections was used for measurement of the coatings thickness and analysis of the coating homogeneity, Fig. 3 and Table 1. Created coatings can be based on SEM analysis considered as uniform and any structural defects were observed in their volume. Therefore the defects observed on the surface of the coatings can be present only in their surface.

Even in the SEM observation, the two layers creating the coating can be easily recognized in the case of the coating prepared for 8 h, Fig. 3c. In the case of shorter treatment time the chemical analysis has to be used for the two layer levels determination.

3.2 Scratch test results

Obtained relationship of acoustic emission and scratch length graphs are given in Figs. 4-6. Micrographs of coatings damage corresponding to the peaks on the plots are included in the graphs.

In the case of the specimen coated for 0.5 h was not possible to specify the damage of the coating from the data obtained during the scratch test, Figs. 4 a-b. However, SEM analysis of the scratch path revealed a large number of small cracks almost in whole the scratch length.

Only the load of 10 N was applied during the scratch test due to the coating damage.

Table 1

Thickness of fluoride conversion coatings prepared at different treatment time.

coating time (h)	0.5	2	8
coating thickness (μm)	0.3	1.7	3.5

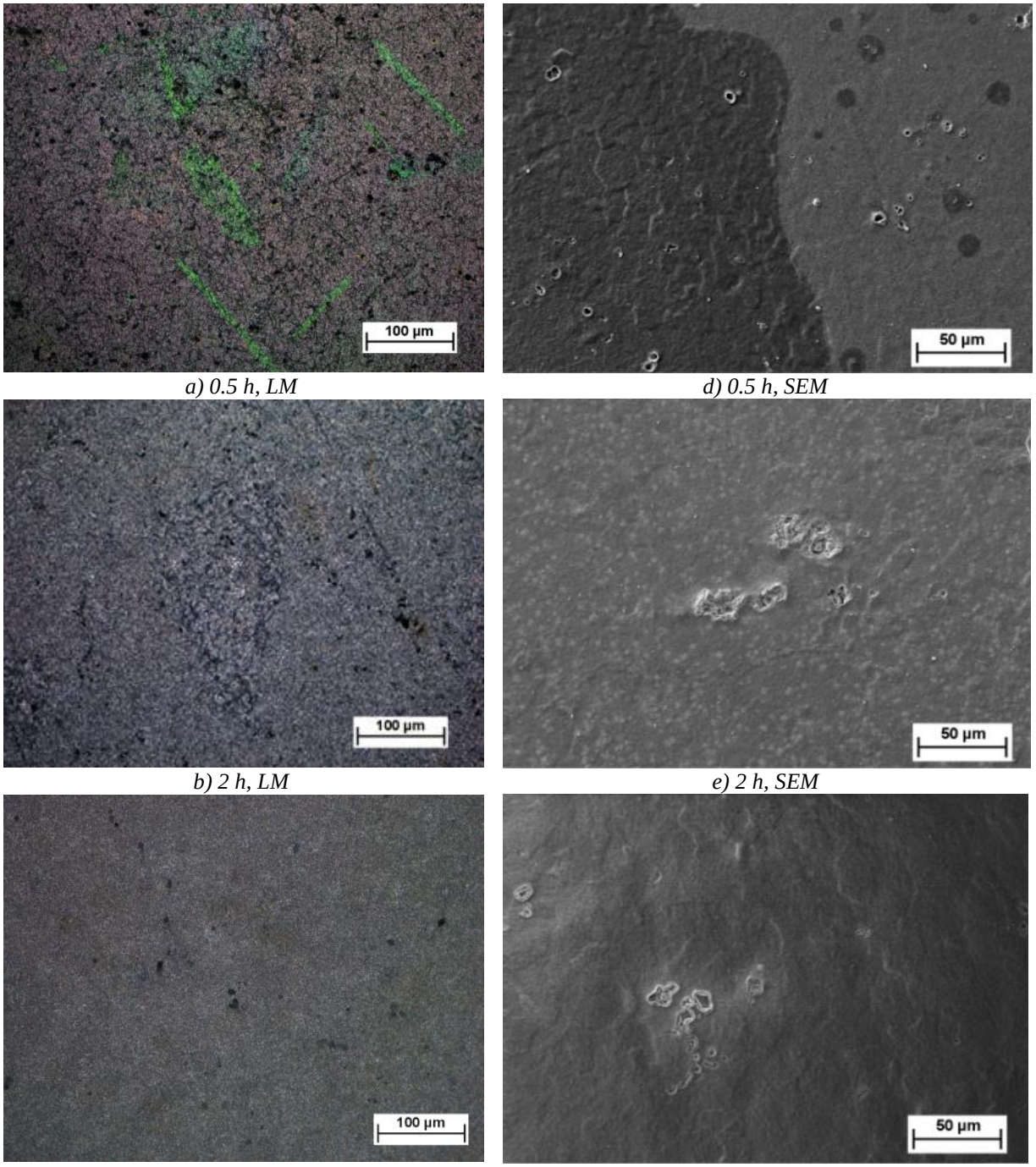

a) 0.5 h, LM *d) 0.5 h, SEM*

b) 2 h, LM *e) 2 h, SEM*

c) 8 h, LM *f) 8 h, SEM*

Fig. 2. Morphology of fluoride conversion coatings prepared at different treatment time.
(full colour version available online)

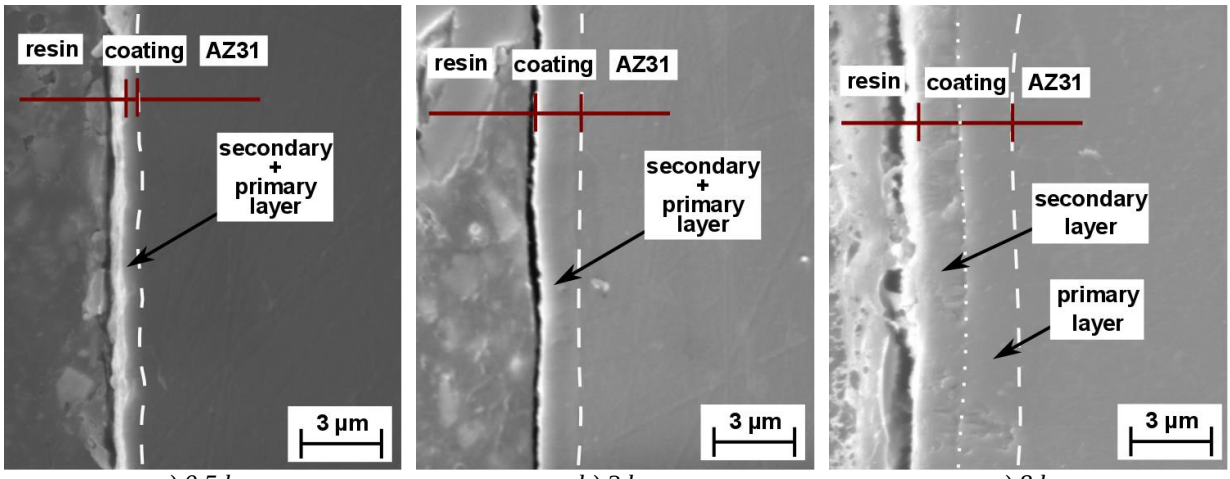

a) 0.5 h *b) 2 h* *c) 8 h*

Fig. 3. Cross section of the coating, SEM.
(full colour version available online)

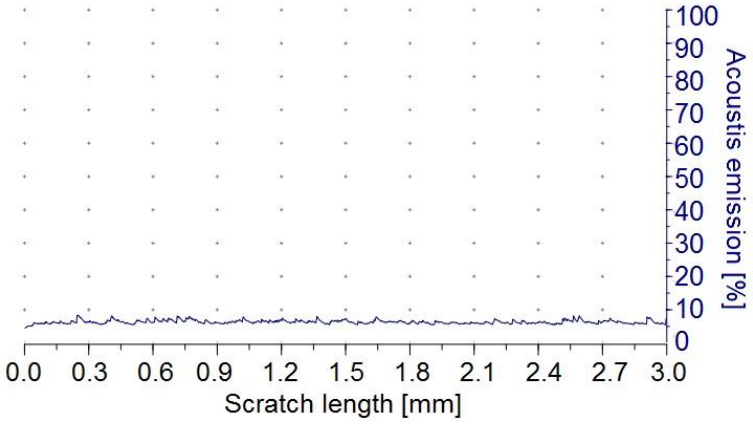

a) acoustic emission

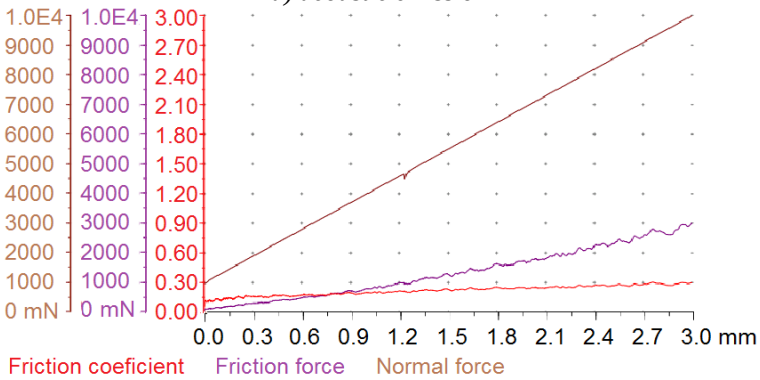

b) normal force and friction

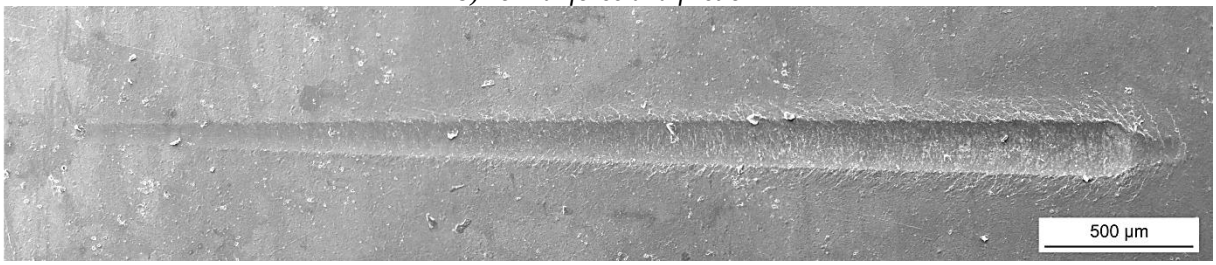

c) scratch detail, SEM

Fig. 4. Acoustic emission vs. scratch length for fluoride conversion coatings prepared at 0.5 h exposure.
(full colour version available online)

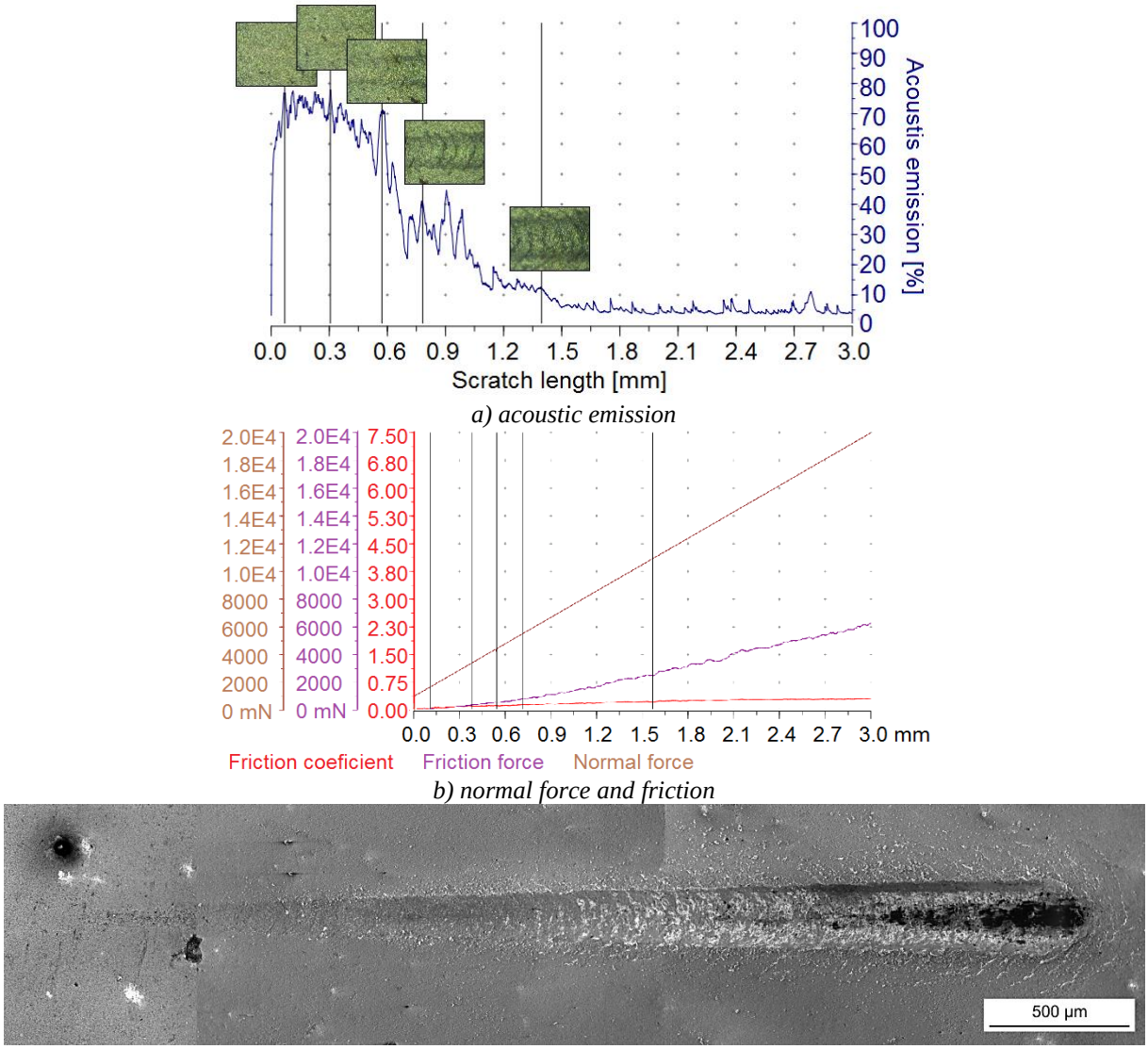

a) acoustic emission

b) normal force and friction

c) scratch detail, SEM

Fig. 5. Acoustic emission vs. scratch length for fluoride conversion coatings prepared at 2 h exposure. (full colour version available online)

First damage of the coating prepared for 2 h was observed in the distance of approximately 0.3 mm from the scratch start (Figs. 5 a-b), however, first cracks of the coating were observed at the distance of 0.58 mm from the scratch start, Fig. 5c. More pronounced coating cracking was observed at the distance of 0.76 mm from the scratch start. The large amount and high intensity of cracks were observed by increasing the scratch length and adequate loading increase. Cracks perpendicular to the scratch direction were characteristic for coating prepared for 2 h. Basic material was revealed at the end of scratch, Fig. 5c.

First signs of damage to the coating prepared for 8 h were observed in the distance of approximately 0.21 mm from the scratch start, Figs. 6 a-b. Two damage mechanisms were observed during the scratch test in the case of the coating prepared for 8 h, Fig. 6c. Two types of cracks were observed in the scratch. While the first cracks type was observed from the distance of 0.75 mm from the scratch start, the second type of cracking mechanism was characteristics for the scratch from 0.89 mm

from the scratch start, Fig. 6c. Also, in this case, the scratch revealed basic coated material.

From the performed scratch tests the forces necessary for prepared coatings damage were determined for the coatings prepared for 2 and 8 h, Table 2. The coating prepared for 2 h in the molten $Na[BF_4]$ salt exhibited lower resistance against scratching comparing to the more thick coating prepared for 8 h, which can be seen from the comparison of Figs. 5 and 6 and from the Table 2.

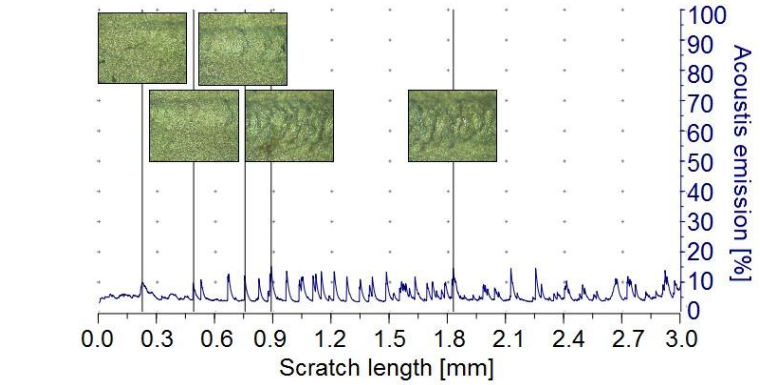

a) acoustic emission

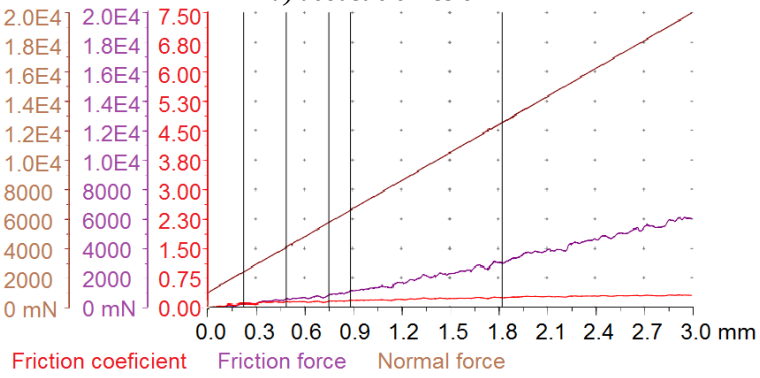

b) normal force and friction

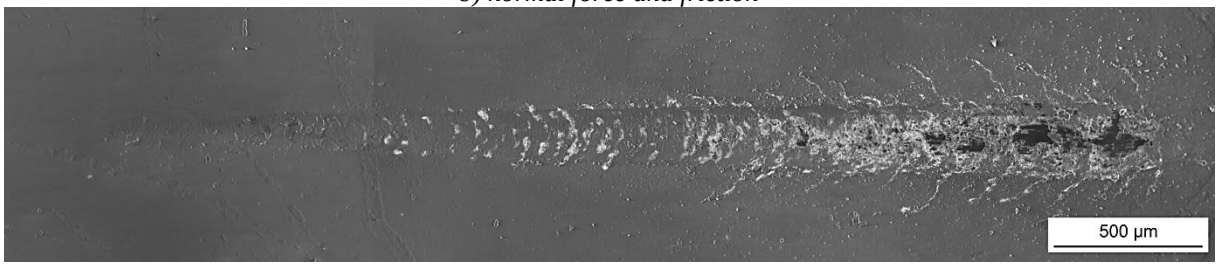

c) scratch detail, SEM

Fig. 6. Acoustic emission vs. scratch length for fluoride conversion coatings prepared at 8 h exposure. (full colour version available online)

Table 2

Coating damaging critical force.

	L_{C1} (mN)	L_{C2} (mN)	L_{C3} (mN)	L_{C4} (mN)	L_{C5} (mN)
2 h coating time	1428	2857	4603	5952	9841
distance from the scratch start (mm) – 2 h	0.09	0.30	0.58	0.76	1.38
8 h coating time	2381	4127	5714	6587	12539
distance from the scratch start (mm) – 8 h	0.21	0.48	0.75	0.89	1.82

4. Discussion

While the fluoride conversion coatings meet the requirements for biomedical applications and increase magnesium alloy corrosion properties, also adhesion properties to the magnesium-based implant should be detrimental for its application for biomedical purposes.

The present study offers a characterization of fluoride conversion coating prepared in $Na[BF_4]$ salt melt at 450 °C. Different treatment times from 0.5 to 8 h resulted in coating creation of an uniform fluoride conversion on polished AZ31 wrought magnesium alloy specimens.

The model explaining the fluoride conversion coating creation from $Na[BF_4]$ salt melt was proposed in [9]. Salt used for conversion coating preparation decompose at 384 °C [9] according to the equation (1):

$$Na[BF_4] \rightarrow NaF + BF_3 \quad (1)$$

Formed BF_3 can react with coated magnesium alloy and form a primary layer of fluoride conversion coating MgF_2 according to the equation (2):

$$3Mg + 2BF_3 \rightarrow 3MgF_2 + 2B \quad (2)$$

Decomposition of the salt is resulting in creation of the primary MgF_2 layer, while a secondary $NaMgF_3$ layer is created over the primary layer simultaneously. The exact mechanism of the primary and secondary layer formation is still not described in the literature.

The coatings prepared in the study uniformly covered the polished AZ31 specimens surface. The local chemical inhomogeneity of the material microstructure (present Al-Mn based intermetallic phase) seems to have no influence on the coating creation even at short treatment times which is in agreement with observations in [9, 11].

Uniform coating coverage of the whole surface of AZ61 wrought magnesium alloy specimens were prepared from Na[BF4] salt at 450 °C treating the material for 2 h was created also in [9] and in [11] using different coating times from 0.5 to 12 h.

A significant increase in the coating thickness was observed by increasing the treatment time from 0.5 to 2 h. Following prolongation of the treatment time led only to smaller thickness increase. This behavior can be explained by the character of coating creation – diffusion + chemical reactions [9].

Comparing to the fluoride conversion coatings prepared from HF solution on AZ61 alloy, no internal defects as microcavities were observed in the coating covering AZ31 alloy. EDS analysis performed in [9] focused on the preparation of the unconventional fluoride conversion coating in the salt melt on AZ61 for 2 h showed compact coverage of the substrate and authors supposed that the defects are only on the surface of the coating. The coatings uniformity was characteristic for all the coatings prepared at different treatment times.

Even though defects were observed on the coating surface, the cross-section of the coating showed the fluoride conversion coating does not contain any defect in the volume. The observation of defects on the surface and no defects in the coating volume can be explained by the assumed diffusion mechanism of the coating creation. This mechanism indicated the growth of the coating into the material volume, which explains no defect in the coating volume. While the coating surface defects can be attributed to the products of chemical reactions playing role on the substrate surface during coating and imperfections of the substrate surface (scratches, impurities, etc.). Even though the diffusion mechanism is assumed for the coating preparation (the mechanism is still not described), the coating has different mechanical properties when compared to AZ31. Applied

loading resulted in coating layer damage, while the damage character was shown to be influenced by the coating thickness.

Treatment time of 0.5 h in the $Na[BF_4]$ salt melt at 450 °C resulted in the coating with the thickness of 0.3 μm. Scratch test indenter penetrated the coating immediately at the beginning of the experiment. No significant damage was observed on the coating surface, while the coating was pushed/introduced to the coated magnesium alloy and a large number of small cracks were observed on the whole scratch length. Mainly the AZ31 magnesium alloy characteristics can be assumed to be measured with the scratch test due to the very low thickness of the coating.

The coating prepared for 2 h with the thickness of 1.7 μm was resistant to the indenter loading until 0.3 mm from the scratch start, where the first coating failure was observable by microscope. This distance corresponds to the load of 2857 mN. A load of approximately 4603 mN corresponding to the distance of 0.58 mm from the scratch was a limit for coating damage. The character of the cracks present in the coating prepared for 2 h corresponds to tensile cracking [12]. Following, an increase of loading resulted in more pronounced coating cracking, however, no cracking mechanism change was observed on the coating surface. At the distance of 0.8 mm from the scratch start corresponding to the loading of approximately 5.8 N the indenter reached a depth of almost the thickness of the coating. Over the distance of 1.5 mm from the scratch start the basic material was reached by the indenter and it can be seen also on the coated material surface after the scratch test, Fig. 5.

While at first the tensile cracks [12] were observed in 0.75 mm from the scratch start, hertz cracking [12] was characteristics for the scratch from 0.9 mm form the scratch start, Fig. 6c, for the coating prepared for 8 h. the change of the damaging mechanism comparing to the coating prepared for 2 h is connected with increased coating thickness. A thick layer of the coating was more resistant to tensile cracking; however, the increasing loading resulted in the creation of larger cracks due to the thicker coating. Scratch test revealed a homogenous response of the coated material for whole the measurement which assumes the stable material resistance against wear.

4. Conclusions

Unconventional fluoride conversion coating was prepared on wrought AZ31 magnesium alloy by immersion in $Na[BF_4]$ molten salt at 450 °C for 0.5, 2 and 8 h. Based on the performed analysis a test the following conclusion can be concluded:

- The coatings prepared in $Na[BF_4]$ molten salt for different times fully covered the AZ31 magnesium alloy but some defects can be observed on the surface. The SEM analysis of the coated specimens cross-section showed that the coating is uniform and any structural defects in their volume were not observed.

- The thickness of the compact fluoride conversion coating increased with increasing coating time.

The results of the scratch tests showed that the wear resistance of the coated material was improved with increasing coating time.

Acknowledgements

This work was supported by Project Nr. LO1211, Materials Research Centre at FCH BUT-Sustainability and Development (National Program for Sustainability I, Ministry of Education, Youth and Sports of the Czech Republic). The research was conducted in the frame of IPMinfra supported through project No. LM2015069 of MEYS.

References

[1] M.P. Staiger, A.M. Pietak, J. Huadmai, G. Dias: Biomaterials 27 (2006) 1728-1734.

[2] H. Baker: ASM Specialty Handbook: Magnesium and Magnesium Alloys, ASM International, 1999.

[3] R.-C. Zeng, J. Zhang, W.-J. Huang, W. Dietzel, K.U. Kainer, C. Blawert, W. Ke: Transactions of Nonferrous Metals Society of China 16 (2006) 763-771.

[4] F.I. Wolf: Molecular Aspects of Medicine 24 (2003) 3-9.

[5] T.S.N. Sankara Narayanan, I.S. Park, M.H. Lee: Journal of Materials Chemistry B 2 (2014) 3365-3382.

[6] Z. Li, S. Shizhao, M. Chen, B.D. Fahlman, L. Debao, H. Bi: Mater. Sc. Eng. C 75 (2017) 1268-1280.

[7] N. Li, Y.D. Li, Y.B. Wang, M. Li, Y. Cheng, Y.H. Wu, Y.F. Zheng: Surface and Interface Analysis 45 (2013) 1217-1222.

[8] K.Y. Chiu, M.H. Wong, F.T. Cheng, H.C. Man: Surface and Coatings Technology 202 (2007) 590-598.

[9] J. Drábiková, S. Fintová, J. Tkacz, P. Doležal, J. Wasserbauer: Anti-Corrosion Methods and Materials 64 (2017) 613-619.

[10] A. Yamamoto, T. Terawaki, H. Tsubakino: Materials transactions 49 (2008) 1042-1047.

[11] J. Drábiková, F. Pastorek, S. Fintová, P. Doležal, J. Wasserbauer: Koroze a ochrana materiálu 60 (2016) 132-138.

[12] S.J. Bull: Tribology International 30 (1997) 491-498.

EXAMINATION OF METAL SIDE HEATING OF LAMP JOINT BY CO_2 LASER BEAM

Tamás Markovits[1*], Miklós Berczeli[1]

[1]Department of Automotive Technologies, Faculty of Transport and Vehicle Engineering, Budapest University of Technology and Economics, Műegyetem rkp. 3., Budapest, Hungary.
[*] corresponding author: e-mail: tamas.markovits@gjt.bme.hu, tel: +3614633468

Resume
Nowadays the vehicle industry is focusing on making materials and technologies for automotive parts that satisfy the newest requirements. Reduction of the manufactured vehicle's weight is such a requirement. There exist many solutions to satisfy this requirement. One of them is when hybrid materials is combined and fixed together. In this research some aspects of the hybrid joining process of steel and PMMA sheet were investigated. Due to the non-transparent type joining CO_2 laser were applied from the metal parts and the laser power and the speed of spot movement were changed in order to roughly determine the process window. In case of adhesive based joining the surface conditions have high importance on the bond strength, therefore the effect of cleaning and blasting of the metal surface was also examined. To determine the role of the value of clamping force it was also changed in some cases. Tensile tests were carried out and the tearing force and the bonded area were measured. In this way the joint strength was determined in case of different setting. New bubble formation was also detected during the process.

Article info
Article history:
Received 23 September 2017
Accepted 19 October 2017
Online 02 January 2018

Keywords:
Laser;
Hybrid joint;
PMMA;
Plastic-steel;
LAMP.

Available online: http://fstroj.uniza.sk/journal-mi/PDF/2017/10-2017.pdf

ISSN 1335-0803 (print version)
ISSN 1338-6174 (online version)

1. Introduction

Reduction of the vehicle weight inspires the development process of the chosen materials and technologies for automotive components. Environmental load and cost efficiency are not only important for the user, but it should be considered during for the whole lifetime, namely from manufacturing to recycling. Considering these aspects the main developing goal can be described, which have given new hybrid material couplings into vehicle industry. Metal-polymer joint is a significant and prevailing technology, which is used in different areas of automotive industry [1]. There are several solutions to join the metal and polymer parts, for example glue, rivets, bolts, but a new innovative technology could be if the concentrated heat induction is generated with laser beam [2-4, 11]. However due to constructive reasons, it is necessary to heat the metal side, because the polymer side in not less suitable when carbon or glass fibre reinforced plastic is used [5]. Based on literary references and developing trends, the research goal is to create hybrid joints by heating the metal side despite other researches, where the joint were created in the direction of the transparent polymer [6-7]. The hypothesis of this work upon is that by using proper technological settings, sufficient amount of heat will flow through the metal disk to create an adhesive hybrid joint with the polymer. Previous researches of the Department of Automotive Technologies show that good quality joints can be created using PMMA and S235 grade steel [2-3]. The authors investigated the joining process of PMMA plastic sheet and steel pin by laser assisted metal plastic (LAMP) joining [8-10]. In this research, the same PMMA and steel materials were used, because of the previous results, which can be used to comparison. The structure of the hybrid joints were investigated

in the case of different laser settings. The bonding area and ultimate strength of the joints were measured, in order to find out the connection between the joints properties and the laser technical parameters. Quality of the created joints are depending on various parameters, such as the power of the laser beam, the velocity of the feeding, the size of the laser beam spot and the surface preparations and parameters of the joining materials. Any changes in these parameters could modify the heat absorption in the materials and create different joint geometry.

2. Experimental procedure

The used materials were a 2 mm thickness poly-methyl-methacrylate (PMMA) and 1 mm thickness S235 JR grade structural steel. The size of the sheets was 60 x 40 mm. The geometry of the PMMA and steel sheets and the experimental setup can be seen in Fig. 1.

The laser beam was an Oerlicon OPL 1800 continuous wave CO_2 gas laser with a maximal 1800 W laser beam power. The diameter of the laser beam was 8 mm on the top surface of steel sheet. The power distribution of the laser beam was TEM_{00}. The laser beam was moved in the clamping device's gap of 30 mm length with a CNC table. Nitrogen gas was used as shielding gas with a flow rate of 5 liter/min to protect the optical system of the laser and the molten area in the steel sheet. The air pressure in the clamping device was hold for 30 second after the laser treatment.

In order to find out the limits of this new joining technology different laser treatment technological parameters were used. The laser beam power, the feed rate, the clamping air pressure and the surface preparation were changed during the research. The laser beam power was changed from 900 to 1100 W, the feed rate was 100, 200, 300 and 450 mm/min, the clamping air pressure 2, 6 bar and the surface preparation of the steel sheet was sand blasted on all side and one case blasted and cleaned with acetone. In one sample non blasted steel sheet was used. The variations of these parameters can be seen in Table 1.

To analyze the structure of hybrid joints Olympus SZX7 stereo microscope measurements were used. The structure and the geometry of the joints, the bubble ratio in the joint can be investigated from the images. The area of the joints can be determined.

Shear tensile test were carried out in a Zwick Z050 testing machine at a cross-head speed of 10 mm/min. The samples were vertical balanced in the cross-head to avoid the bending effect during the test with an opposite side thickness sheets. The shear strength can be calculated from the area of the joints and the tensile tests results.

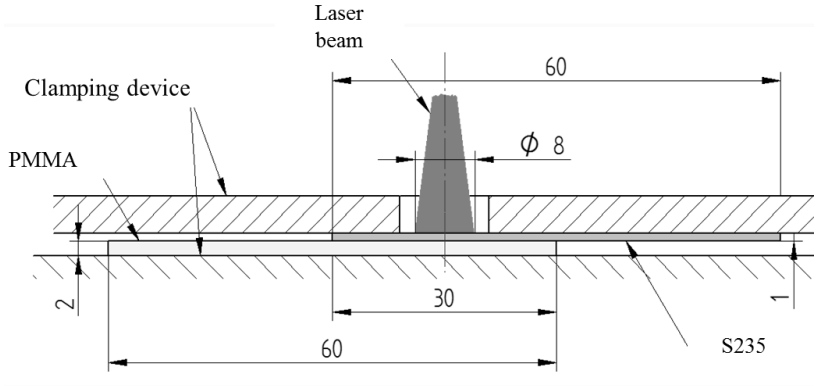

Fig. 1. The geometry of the PMMA and S235 steel sheets and the experimental setup.

Table 1

The used technology parameters.

Laser beam power (W)	900				1100			
Feed rate (mm/min)	10	200	300	450	100	200	300	450
Clamping pressure (bar)	6	6	2	6	6			
Surface preparation	Sand spreaded	Sand + Aceton	Sand spreaded		Sand spreaded			

3. Description of achieved results

In one case, when non blasted steel sheet was used high percent of the laser beam reflected from the surface of the metal part and not formed the bonding.

In Fig. 2 the joints with the smallest and the largest area can be seen. The joint with 900 W laser power and 450 mm/min feed rate has the smallest joint area (Fig. 2a and 2b). The laser beam heating not cause melted pool in the steel, just heat affected zone appeared on the top and bottom side of the S235.

The joint with the 1100 W laser power and 200 mm/min feed rate has the largest joint area (Fig. 2c and 2d). It's because the high laser power and the low feed rate pairing cause the highest heat input into the S235 steel and much more heat can convention to the PMMA sheet. It's important to optimize the heat input, because too much heat can damage the PMMA and the structure of the hybrid joint. Large melted pool can be seen in the S235 structure. Concentric bonding area can be seen in the PMMA structure with the melted pool.

The bonding structures can be seen in Fig. 3. In case of low heat input the centre of the bonding structure contains only small bubbles and the PMMA only melted under the laser spot (Fig. 3a). When the heat input increased in the centre of the bonding appeared a wide gas channel in the PMM (Fig. 3b). Away from the gas channel, large and small bubbles contain the bonding. The gas leaved the channel through ducts on the bottom of the PMMA and exit end the end of the PMMA sheet. The melted area in the PMMA is wider than the 8 mm of diameter laser beam spot.

The Fig. 4 shows the results of the strength calculating with these resolution of laser technology parameters setup. The diagram shows same parabolic trend with maximum points in the results when the same laser power was used. The samples with 900 W laser power and feed rate of 100, 200 and 300 mm/min have higher strength than the 1100 W samples. It could be because of the lower heat input at the 900 W samples. More heat input not always increase the strength of the bond. Too much heat cause damage in the PMMA and not increase the strength of the bonds. The 1100 W samples have the same trend but shifted to right, to the lower heat input zone. 1100 W samples have higher strength with 450 mm/min. The size and number of the bubbles have an optimal ratio, when the strength is the highest. During the tensile test in cases of 28 from 30 the sheets were separated, only in 2 cases were the PMMA broken.

The Fig. 5 shows the effect of the different surface preparation changing on to the shear force. When all side of the S235 steel sheet was cleaned with acetone flow the shear force decreased, the reason could be the acetone cleaning fluid remained microelements after evaporation and these have negative effect for the bonding quality.

In case when the air pressure decreased in the clamping device (Fig. 6) the shear force of the bonding is decreased. Lower clamping force causes lower strength between the S235 steel and PMMA sheets.

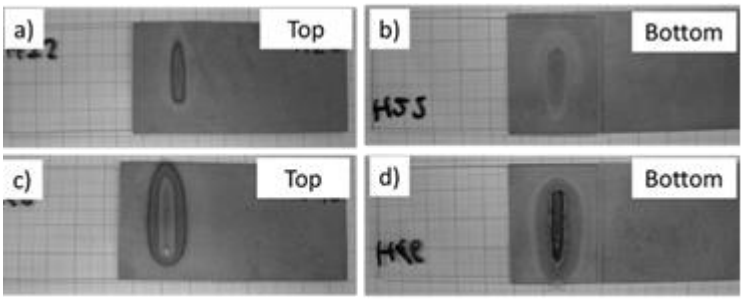

Fig. 2. Top and bottom side of the joints: a) and b): 900 W, 450 mm/min

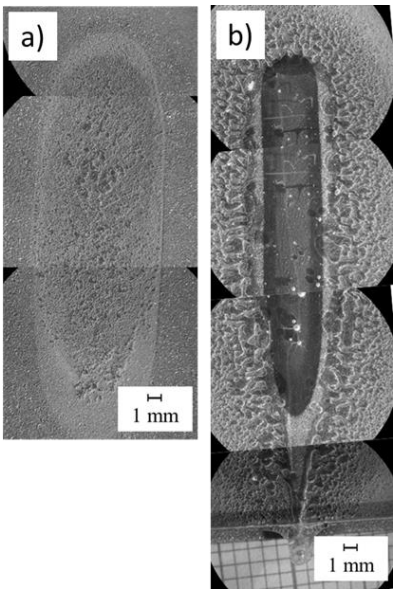

Fig. 3. The microstructure of the joints: a) the smallest area joint: 900 W, 450 mm/min, b) the largest are joint: 1100 W, 200 mm/min.

.

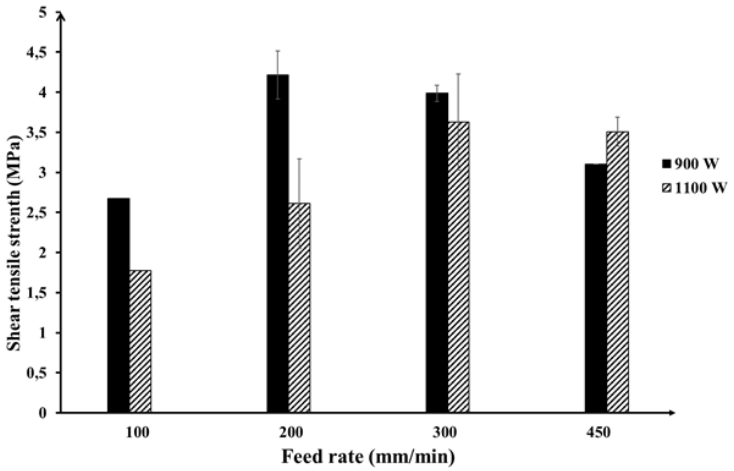

Fig. 4. Compare the 900 and 1100 W samples depending on shear tensile strength and the feed rate. The chart contains the error line for each setup.

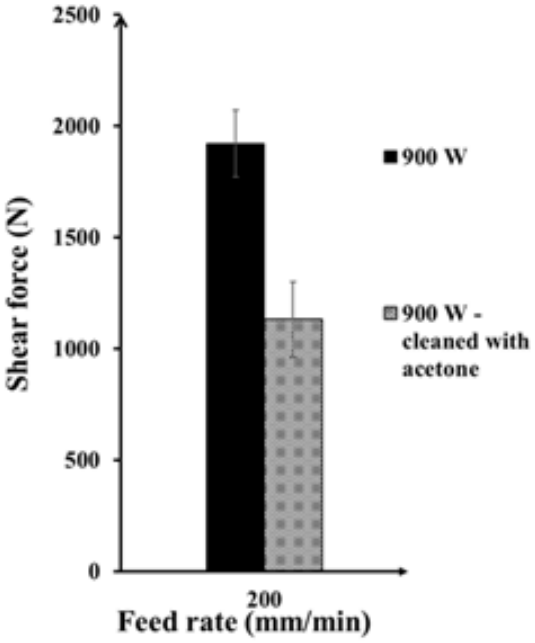

Fig. 5. The effect of the acetone cleaning and changing with 900 W laser power and 200 mm/min setup.

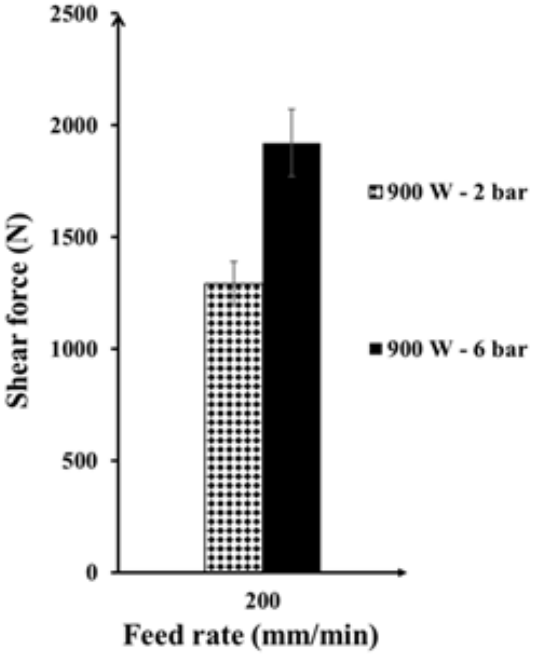

Fig. 6. The effect changing the clamping pressure in the clamping device with 900 W laser power and 200 mm/min setup.

4. Conclusions

In this research, hybrid PMMA and S235 steel sheets joints were created using a continuous wave laser power with CO_2 beam source and different technical parameter setups, the following conclusions can be drawn from this study:

Hybrid joints can be created using laser beam heating to the metal sheet side.

The shear tensile strength has an optimum, depending on the laser power and the speed of laser spot. With 900 W 200 mm/min and wit 1100 W the 300 mm/min has the optimum in case of the applied resolution.

The size and quantity of the bubbles in PMMA have optimum ratio to increase the shear tensile strength.

Sand spreading of the metal sheet increases the strength of the joint because of the higher laser absorption and better adhesion between the plastic and metal parts.

Higher clamping pressure cause higher share strength.

Acknowledgements

The project presented in this article is supported by the ÚNKP-16-2-I. New National Excellence Program of The Ministry of Human Capacities.

References

[1] R. Heuss, N. Müller, W. Sintern: Lightweight, heavy impact, Advanced industries (2012).

[2] T. Markovits, A. Bauernhuber, J. Takács: 33rd International Colloquium on Advanced Manufacturing and Repair Technologies in Vehicle Industry, Ed.: Lenka Kuchariková (2016) 61-64 .

[3] T. Markovits, A. Bauernhuber: Analysis of technology in various industries. Ed: Stanislaw Borkowski, Robert Ulewicz (2014) 17-26.

[4] A. Roesner, S. Scheik, A. Olowinsky, A. Gillner, U. Reisgen, M.s Schleser: Physics Procedia 12(1) (2011) 370-377.

[5] Lamberti, T. Solchenbach, P. Plapper, W. Possart: Physics Procedia 56(1) (2014) 845-853.

[6] A. Bauernhuber, T. Markovits: Physics Procedia 56(1) (2014) 811-817.

[7] K.W. Jung, Y. Kawahito, M. Takahashi, S. Katayama: Materials & Design 47(1) (2013) 179-188.

[8] M. Wahba, Y. Kawahito, S. Katayama: Journal of Materials Processing Technology 211(6) (2011) 1166-1174.

[9] T. Markovits, A. Bauernhuber: Scientific papers ot the University of Pardubice: Series B. (2015) 89-98.

[10] S. Katayama, Y. Kawahito: Scripta Materialia 59(1) (2008) 1247-1250.

[11] E. Tillova; L. Kucharikova, M. Chalupova, J. Belan, A. Vaško, I. Švecová: Metalurgija 56(1-2) (2017) 47-50.

EXAMINATION AND POLISHING OF SURFACE SCRATCHES ON HANDHELD DEVICES

József Hlinka[1*], Zoltán Pál[1], Krisztián Bán[1], Andor Bauernhuber[1]

[1] Department of Automotive Technologies, Faculty of Transportation and Vehicle Engineering, Budapest University of Technology and Economics, Stoczek u. 6, 1111 Budapest,. Hungary
[*] corresponding author: e-mail: jozsef.hlinka@gjt.bme.hu, jozsefhlinka@gmail.com , tel: +36304827169

Resume
Pollution is a current environmental problem. Personal used mobile phones and devices with LCD displays are often thrown away only the optical matter. The renewal of these device surfaces is at the focus of common interest. Our examination was a well-defined micro-scratch test using a special microhardness and scratch tester equipment (MCT). This equipment provides four different means of analyzing the scratch: acoustic emission detection, tangential force measurement, scratch depth measurement, optical observation through a digital microscope. The scratches were made with normal force from 0.5 to 15 N, the same length (20 mm) with the same diamond indenter. The scratches were analyzed with contact and non-contact methods, laser surface topographical analysis, optical microscopic examination, and surface roughness testing. On the LCD display we created specified scratches with the MCT scratch tester and after these scratches had to be repaired by polishing. Three different polishing speeds and loads were used. The measured wear rates show that higher polishing loads result increased wear rates but this trend does not true for the polishing speed.

Available online: http://fstroj.uniza.sk/journal-mi/PDF/2017/11-2017.pdf

Article info
Article history:
Received 23 August 2017
Accepted 19 October 2017
Online 02 January 2018

Keywords:
scratch test;
LCD display;
surface roughness;
polishing;
scratch depth.

ISSN 1335-0803 (print version)
ISSN 1338-6174 (online version)

1. Introduction

Nowadays pollution is one of the highest environmental problem. The handheld devices which are used in everyday life are often thrown away because of the scratches on the surfaces and other optical defects of the surfaces. There is at the heart of common interest to renew these device surfaces. A lot of personal handheld device become unusable and rubbish because of the scratches on the screen. Polishing could be a possible way of repairing scratched surfaces of handheld devices. With our examination we want to investigate the properties of the scratches like scratch depths and which method is the best choice for the examination of scratched surface and compare scratches which created by unknown loads with scratches which made by definite loads. After scratches were made we measured how the scratched surfaces can be repaired with polishing.

2. Materials and methods

Three different parts of handheld devices were analyzed, LCD panel, phone display, and phone cover (Fig. 4.). There are scratched samples, when the scratches created by unknown loads. And there is a part of the measurements when the analyzed scratches made by predefined loads.

2.1 Laser surface profilometer

The surface topography was mapped using an optical sensor within a Rodenstock RM600 surface-measuring instrument. The optical sensor maps the topography of the surface using a laser beam, which is focused on the surface (Fig. 1. a, b). The sample is moved by a CNC table under the optical sensor, enabling automatic scan above the pre-assigned areas. After the scan of the measured area the 3D topography can be sectioned along any line

and with this sectional profile the surface roughness characteristics and distance of various points of the profile can be calculated.

2.2 Surface roughness analyzer

The Mitutoyo Surftest 301 can measure a 2D profile of the measured surface using piezo electric principle. The device pull a diamond probe-tip across the surface to be measured, and record the vertical displacement of the probe-tip with the function of the horizontal displacement (Fig. 1. c). From the detected profile points the device calculates the characteristics of the surface roughness (Ra, Rz, Rmax).

2.3 CSM Micro Combi Tester

The CSM Micro Combi Tester (MCT) is a special microhardness and scratch test equipment which is widely used for scratch examination [1, 2]. The scratches with predefined load parameters were made by CSM MCT machine. The MCT measures the Ft shear force which is parallel to the displacement, the acoustic emission and the tip penetration depth into the sample. The indenter is lowered onto the sample surface. After reaching a low contact load (0.1 N) defined by the user, the table moves with a constant speed and scans the surface. After the scan, the machine makes a scratch with a load defined by the user. After this step the machine makes another scan from the surface with a low contact load (0.1 N). The residual depth is the difference between the scan before and after the scratch production. The residual depth characterizes the scratch. The scratches were made by a Rockwell indenter with tip radius of 0.05 mm. An example of the measurement was shown in Fig. 2.

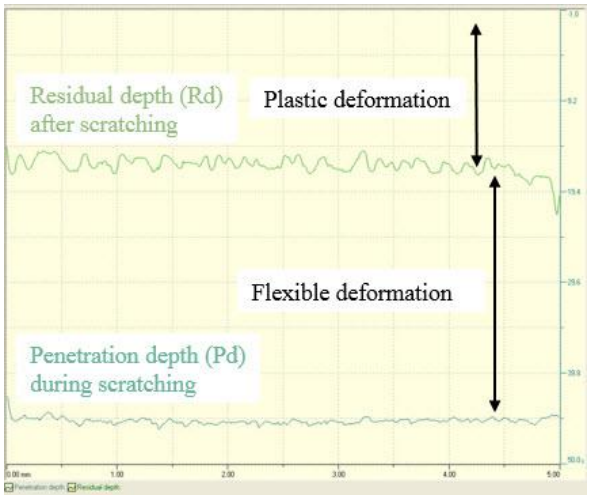

Fig.2 Measurement sample of CSM Micro Combi Tester (LCD panel sample, 5 N scratch making load).
(full colour version available online)

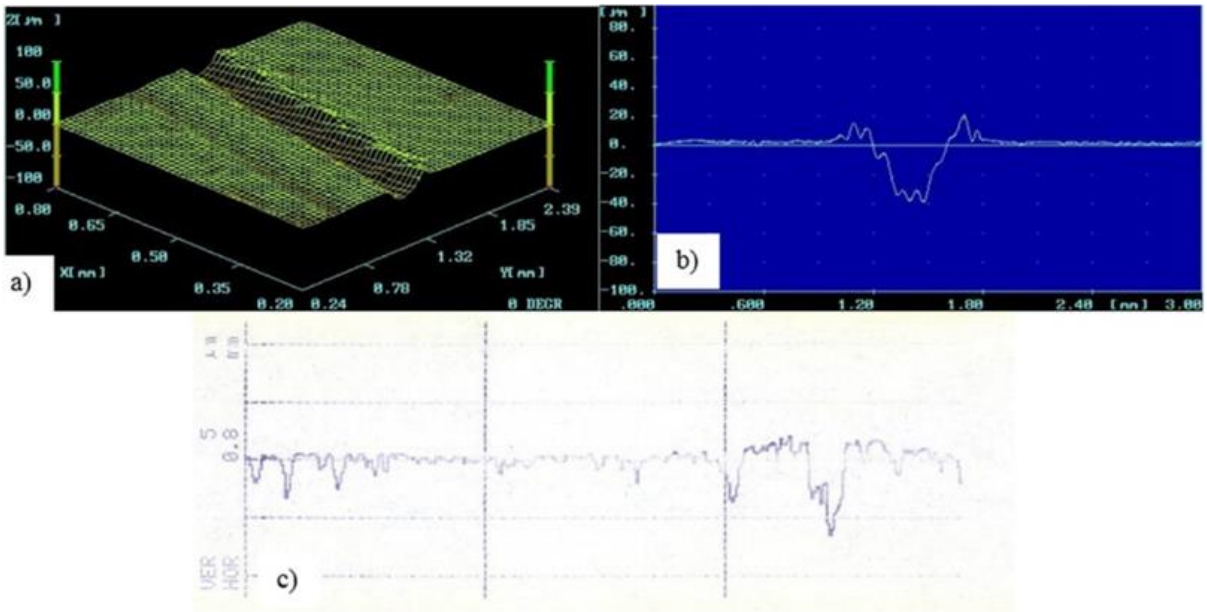

Fig.1 Scratch analyzed on Line D with RM600 laser surface profilometer (a and b) and Mitutoyo Surftest 301 surface roughness analyzer (c).
(full colour version available online)

2.4 Buehler Beta grinder-polisher machine

The polishing operation was performed on a Buehler Beta grinding and polishing machine (Fig. 3.). The speed of the polishing machine can be controlled, and with the Buehler Vector LC Power Head, we can set different loads to push the sample to the polishing cloth. Polishing operations were performed with 3μm diamond polishing liquid.

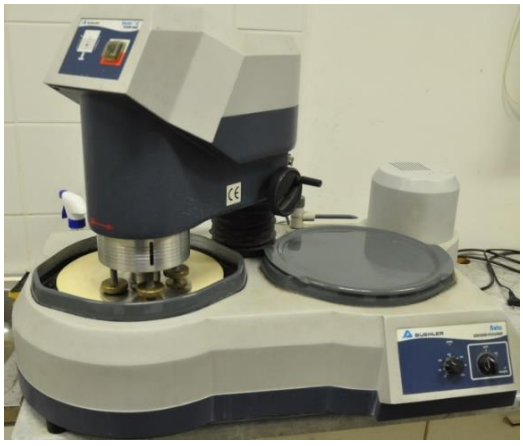

Fig.3 Buehler Beta grinder-polisher machine.
(full colour version available online)

3. Results and discussions

3.1 Scratches with unknown load of creation

The scratches, when the force of creation was not defined, are shown in Fig. 4. The measured points of the samples are marked. All of the scratches are visible to the unaided eye. The scratches length (up to 80mm) and depth (up to 70 μm) are different. The scratches were shot with a camera with macro objective, but the photographs were not enough to analyze the scratches. Scratches which made by unknown force were analyzed by contact and non-contact surface topography measurements.

Fig. 5. shows the measured scratch depths created by unknown loads. The smallest scratch of the LCD panel was not detectable with RM600 device. The scratches of the phone display were not detectable with the contact and non-contact method. The reason is that the depth of the scratches are very small, barely noticeable, and the laser beam is not, or only very weakly reflected from the glass surface, which makes laser measurement impossible. The results show, that measurements with the stylus tip almost in all cases show higher scratch depths. On the edge of the scratch there is protruding material because of the plastic deformation, and the maximum vertical distance between the profile points are always higher than the distance between the bottom of the scratch and the original surface plane. If the surface material allows, it is practical to measure the scratches with the RM600 surface-measuring instrument.

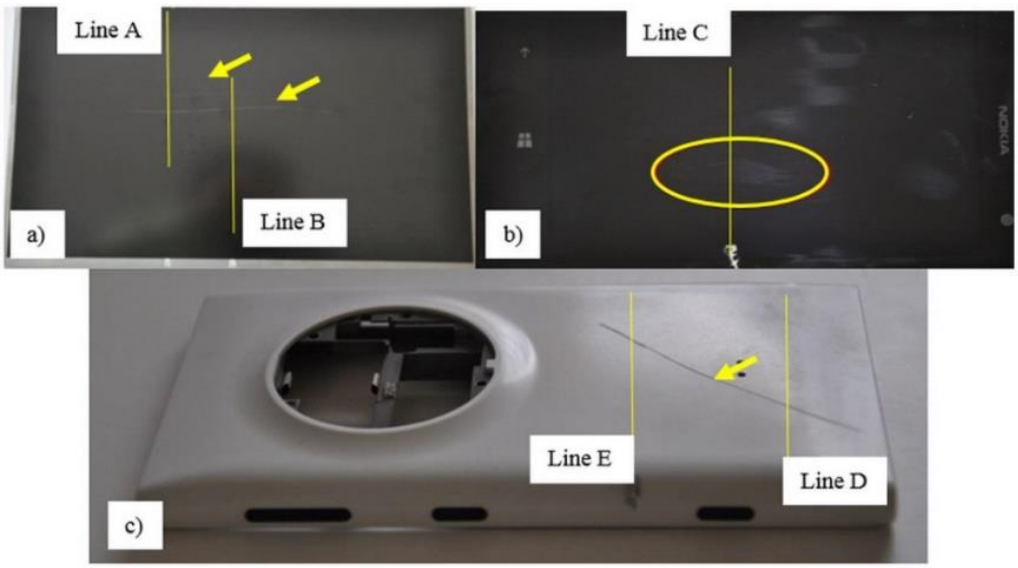

Fig. 4 Scratched a) LCD panel, b) phone display, c) phone cover.
(full colour version available online)

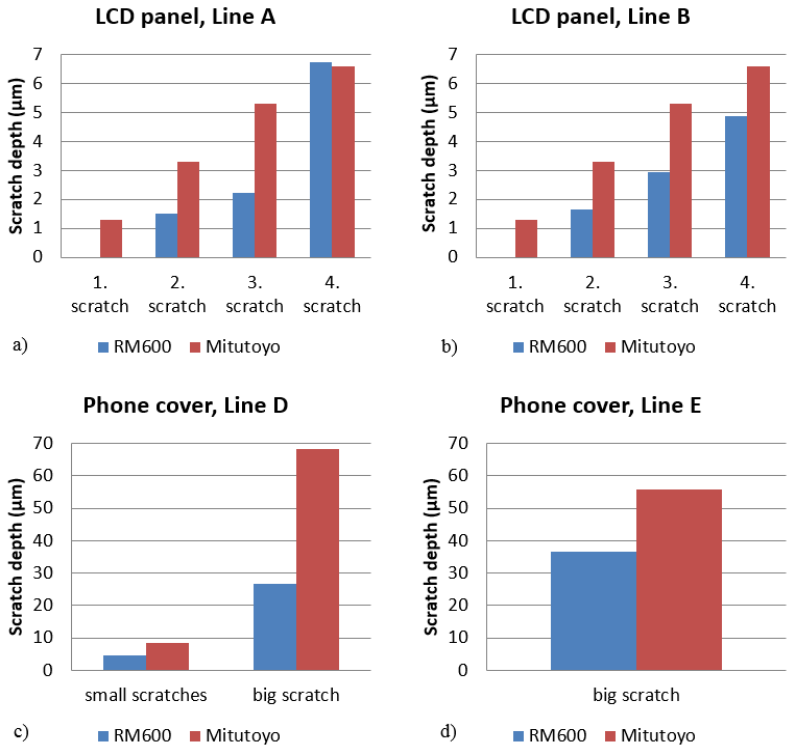

Fig. 5 Scratch depths created by unknown loads, measured with RM600 and Mitutoyo Surftest 301.
(full colour version available online)

3.2 Scratches with definite load of creation

In case of the LCD panel and the phone display the smallest scratch, created by the smallest 0.5 N load, cannot be detectable with the RM600 and the Mitutoyo contact surface roughness tester. When the loads were higher the scratches were well definable. By optical microscope and surface topography measurements it was stated that plastic deformation dominates during scratches of LCD panel and phone cover. The missing material from scratch tracks made peaks at the edge of scratch valley. In case of phone display, which is a rigid glass, the plastic deformation was not typical during scratch tests. The missing material from the scratch tracks was pitting out, and could be removed from the surface as a glass powder after scratching (Fig. 6.).

The diagrams in Fig. 7. shows the measured scratch depths versus the load. Scratch depths were measured with MCT, RM600 and Mitutoyo Surftest 301. To get the average scratch depth of a scratch, measurements were performed in 3 different points of the sample. The diagrams show the average scratch depths and the deviations in each measuring method. The results show that higher loads result deeper scratches. In case of LCD panel and phone cover the scratch depths increases monotonically. If phone display was examined between 5-8 N loads the scratch depths were not change and at 10 N load increased significantly. This phenomenon can be explained by the rigidity of glass. When the load was 15 N the scratch depths became deeper on the glass surface. In case of LCD panel and phone cover the deviation of the results are low the measurements are well repeatable.

In case of scratches created by the highest load the Mitutoyo contact surface roughness tester measured the largest scratch depths. This is because the deepest scratch tracks create the highest protrusion, burr and this method adds this height to the scratch depth. An exception to this is the phone display because of the pitting the scratch depth are not even. In some points the scratch is deeper than the average depth.

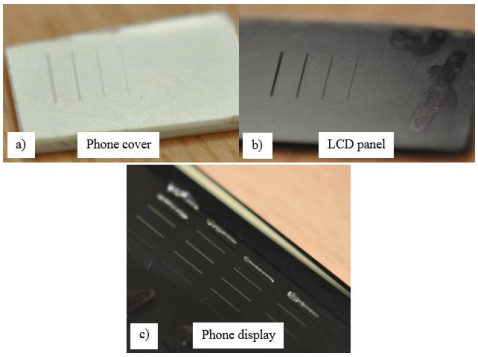

Fig.6 Scratch depths created with known loads, measured with MCT, RM600 and Mitutoyo Surftest 301.
(full colour version available online)

3.3 Polishing of surface scratches

Before the polishing process we measured the scratch depth with Mitutoyo Surftest 301 surface roughness analyzer. Then the samples were placed in the polishing machine and the load settings were adjusted. The scratches of the samples were perpendicular to velocity vector of the polishing cloth. We selected 1 minute intervals for the cycle of polishing and scratch depth measurement. The scratch depths were measured in 5 points and using the average value for further evaluation. The evaluation was performed only for the two deeper scratches because the results of the smallest scratches could not be evaluated properly.

The predefined loads during the polishing were N_1 = 10 N; N_2 = 30 N; N_3 = 50 N. The samples were polished in different positions so the distance between the sample position and the center of the rotating polishing cloth resulted different polishing speeds. The distance between the center of rotation and the samples were d_1 = 30 mm; d_2 = 80 mm; d_3 = 120 mm. The revolution was 200 1/min. The polishing speeds were v_1 = 0.6283 m/s; v_2 = 1.6755 m/s; v_3 = 2.5133 m/s.

For each polishing setting a steady-state wear rate can be easily identified. A straight line can be fitted to the measuring points and the slope of the line represents the wear rate.

The measured wear rates on LCD panel samples were collected in Table 1. It can be seen from the table that lower wear rates can be measured in case of smaller scratches. Clearly visible that the increasing loads increase wear rates too, but on the other hand polishing speeds changes the wear rates differently.

The maximum wear rates were measured at v_2 speed. Of course, this does not mean that this speed gives the expected optimum. But the speed which generates the maximum wear rate could be found with a proper resolution experiment around v_2 speed.

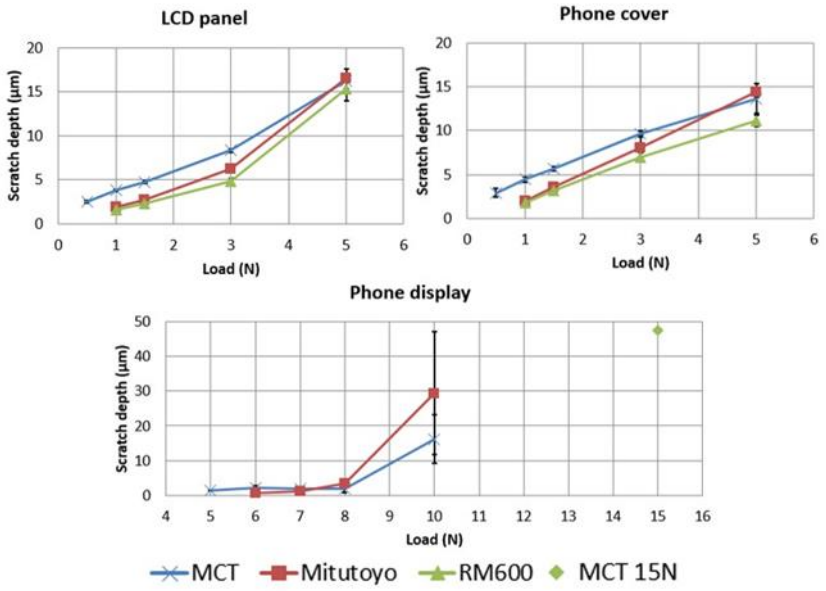

Fig.7 Scratch depths created with known loads, measured with MCT, RM600 and Mitutoyo Surftest 301.
(full colour version available online)

Table 1

Wear rates on LCD panel samples

		N_1	N_2	N_3
v_1	2. scratch (3 N load)		0.6062 μm/min	
	3. scratch (5 N load)		0.9146 μm/min	
v_2	2. scratch (3 N load)	1.3800 μm/min	2.9842 μm/min	3.5743 μm/min
	3. scratch (5 N load)	2.6314 μm/min	3.2556 μm/min	4.7200 μm/min
v_3	2. scratch (3 N load)		1.8392 μm/min	
	3. scratch (5 N load)		1.9517 μm/min	

4. Conclusion

According to the results we can say that the results of MCT is acceptable the best, because the instrument can calculate the depth of the scratch from the scratch tip vertical displacement during the scratch track scanning. If we have to define the depth of an existing scratch the RM600 is recommended because it measures with non-contact method and does not cause other deformations during the measurement process. If the sample surface cannot be measured with laser topography the contact surface roughness measurement could be the solution.

The scratch polishing results in case of LCD panel show that increasing polishing load increase the wear rate. On the other hand the maximum of wear rate is not at the highest polishing speed. The optimal polishing speed is around v_2 speed.

Acknowledgements

This research has been supported by the grants of the Highly Industrialized Region in Western Hungary with limited R&D capacity: "Strengthening of the regional research competencies related to future oriented manufacturing technologies and products of strategic industries by a research and development program carried out in comprehensive collaboration", under grant No. VKSZ_12-1-2013-0038.

References

[1] R. Fábián, M. Furkó, B. Vehovszky. XIX. Scientific Session of Young Engineers XIX. International Scientific Conference, Cluj-Napoca (2014) 145-148.

[2] Z. Pál, A. Lovas. Measuring attributes of thermopower and hardness measurement of glassy alloys. Perner's Contact 6 (2) 221-227.